Assessment of Southern Ocean mixed-layer depths in CMIP5 models: Historical bias and forcing response

Article *in* Journal of Geophysical Research: Oceans · April 2013

DOI: 10.1002/jgrc.20157

6 authors, including:

Jean-baptiste Sallée
Pierre and Marie Curie University - Paris 6
40 PUBLICATIONS **862** CITATIONS
SEE PROFILE

Emily Shuckburgh
British Antarctic Survey
43 PUBLICATIONS **1,293** CITATIONS
SEE PROFILE

Andrew Meijers
British Antarctic Survey
21 PUBLICATIONS **428** CITATIONS
SEE PROFILE

Assessment of Southern Ocean mixed-layer depths in CMIP5 models: Historical bias and forcing response

J.-B. Sallée,[1] E. Shuckburgh,[1] N. Bruneau,[1] A. J. S. Meijers,[1]
T. J. Bracegirdle,[1] and Z. Wang[2]

Received 1 August 2012; revised 27 February 2013; accepted 7 March 2013; published 9 April 2013.

[1] The development of the deep Southern Ocean winter mixed layer in the climate models participating in the fifth Coupled Models Intercomparison Project (CMIP5) is assessed. The deep winter convection regions are key to the ventilation of the ocean interior, and changes in their properties have been related to climate change in numerous studies. Their simulation in climate models is consistently too shallow, too light and shifted equatorward compared to observations. The shallow bias is mostly associated with an excess annual-mean freshwater input at the sea surface that over-stratifies the surface layer and prevents deep convection from developing in winter. In contrast, modeled future changes are mostly associated with a reduced heat loss in winter that leads to even shallower winter mixed layers. The mixed layers shallow most strongly in the Pacific basin under future scenarios, and this is associated with a reduction of the ventilated water volume in the interior. We find a strong state dependency for the future change of mixed-layer depth, with larger future shallowing being simulated by models with larger historical mixed-layer depths. Given that most models are biased shallow, we expect that most CMIP5 climate models might underestimate the future winter mixed-layer shallowing, with important implications for the sequestration of heat, and gases such as carbon dioxide, and therefore for climate.

Citation: Sallée, J.-B., E. Shuckburgh, N. Bruneau, A. J. S. Meijers, T. J. Bracegirdle, and Z. Wang (2013), Assessment of Southern Ocean mixed layer depths in CMIP5 models: Historical bias and forcing response, *J. Geophys. Res. Oceans*, *118*, 1845–1862, doi:10.1002/jgrc.20157.

1. Introduction

[2] The mixed layer at the surface of the ocean is the gateway for all exchanges between the air and the sea. This role as a gateway is especially relevant in the Southern Ocean, where intense winds and extreme buoyancy fluxes create some of the thickest mixed layers on Earth [*de Boyer et al*., 2004]. These deep mixed layers provide a conduit for the sequestration of heat and gases (including carbon dioxide) from the atmosphere into the ocean's interior [*Sabine et al.* 2004; *Ito et al.*, 2010; *Sallée et al.*, 2012]. Thus, it is important to assess how well the Southern Ocean mixed layer is represented in climate models since it can affect the accuracy of future projections.

[3] The deepest mixed layers of the Southern Ocean form directly north of the Antarctic Circumpolar Current (ACC) in winter [e.g., *McCartney*, 1977; *Sallée et al*., 2006; *Dong et al*., 2008]. In this circumpolar band of thick mixed layer, mode and intermediate waters acquire their physical and biogeochemical properties before being subducted into the interior ocean. These waters then ventilate the thermocline of the Southern Hemisphere subtropical gyres [*Sallée et al*., 2010a]. Due to their large thickness and their surface formation, mode and intermediate waters have long been recognized as key water masses for determining the global distribution and budgets of heat, carbon and nutrients [e.g., *Sarmiento et al*., 2004; *Sabine et al*., 2004; *Ito et al*., 2010; *Sallée et al*., 2012]. In particular, estimates suggest that more than 40% of the total oceanic anthropogenic carbon has entered the ocean south of 40°S. In addition, there are indications from paleoclimatic records that a breakdown in stratification in the Southern Ocean contributed to the rise of atmospheric carbon dioxide at the end of the Last Glacial Maximum [*Toggweiler and Russell*, 2008; *Anderson et al*., 2009]. This emphasizes the importance of accurately representing the Southern Ocean mixed layer in order to accurately model past, present and future climate.

[4] Climate models of the third Coupled Model Intercomparison Project (CMIP3) exhibited wide variation in their ability to represent deep winter mixed layer in the Southern Ocean [*Downes et al*., 2009, 2010]. Since then, various improvements have been suggested to the parameterization of mixed layer dynamics, some of which have been implemented in the models contributing to the Coupled Model Intercomparison Project Phase 5 (CMIP5).

[1]British Antarctic Survey, Cambridge, UK.
[2]School of Marine Sciences, Nanjing University of Information Science and Technology, Nanjing, China.

Corresponding author: J.-B. Sallée, British Antarctic Survey, High Cross, Madingley Road, Cambridge CB30ET, UK. (jbsallee@gmail.com)

2169-9275/13/10.1002/jgrc.20157

Perhaps the most significant characteristic of the ocean mixed layer, in contrast to the atmospheric boundary layer, is the presence of surface waves, which result in both wave breaking and Langmuir circulation at the free surface [*Noh and Min*, 2004]. A number of turbulent kinetic energy closure schemes have been developed to parameterize this complex physics, which is associated with mixed layer convection and restratification. New-generation turbulence closure schemes have been implemented in some CMIP5 models (e.g., IPSL group, J. L. Dufresne et al., Climate change projections using the IPSL CM5 Earth System Model: From CMIP3 to CMIP5, submitted to *Climate Dynamics*, 2012), with representation of double diffusion processes [*Merryfield et al.*, 1999], Langmuir cells [*Axell*, 2002] and surface wave breaking [*Mellor and Blumberg*, 2004; *Burchard and Rennau*, 2008]. In addition, the restratification effects of the finite-amplitude, sub-mesoscale mixed layer eddies are included in some models [e.g., CCSM4 group, *Danabasoglu et al.*, 2012] using the mixed layer eddy parameterization of *Fox-Kemper et al.* [2008] as implemented by *Fox-Kemper et al.* [2011]. Other model developments might also be expected to improve the representation of the mixed layer. *Lee et al.* [2011] showed that increased model resolution can improve the representation of the ocean advection of buoyancy and the stratification in the Southern Ocean, which translates into a much more realistic mixed-layer representation. Improvements that have been made to the representation of fluxes of heat, freshwater and momentum at the air-sea interface, either through improvements to the atmospheric models or to the atmosphere-ocean coupling, might also be expected to benefit the representation of the ocean mixed layer. The Southern Hemisphere surface winds have also a strong impact on the mixed layer in the Southern Ocean [e.g., *Sallée et al.*, 2010b] and they have been shown to be influenced by the representation of ozone recovery during the first half of the 21st century [*Son et al.*, 2008, 2010]. Unlike CMIP3, all CMIP5 models include a representation of stratospheric ozone changes (see information about ozone forcing in *Bracegirdle et al.* [2013]; we note that not all models use the same ozone forcing, and thus, the effect may be of different intensity in the different models).

[5] In this paper, we assess present-day skill and projected changes simulated by the CMIP5 models, focusing on the Southern Ocean mixed layer. To date, no study has consistently analyzed the causes of present-day Southern Ocean mixed-layer bias in climate models, despite the fact that 10 years of Argo profiles in the Southern Ocean now give us a robust understanding of the structure, characteristics and formation of the real Southern Ocean winter mixed layer [*Dong et al.*, 2008; *Sallée et al.*, 2010b]. Here, we present such a consistent analysis. A detailed study of the influence of particular parameterization schemes used in different models is beyond the scope of this paper, however, we do attempt to identify the most important forcings leading to biased representation. Turning to future projections, we provide a summary of the multi-model projections and examine whether there is a state dependence in the model response. Due to their importance for climate, we focus our analysis on the assessment of the deep mixed-layer band developing in winter and leading to the formation of mode and intermediate water. The implications of mixed layer representation for modelled mode and intermediate water masses are tackled at the end of the paper, and are further discussed in the framework of the Southern Ocean overturning circulation in a companion paper [*Sallée et al.*, 2013].

2. Data and Methods

2.1. CMIP5 Models and Observation-Based Products Used in the Assessment

[6] Climate model outputs run for CMIP5 [*Taylor et al.*, 2012] are assessed in this study, including both atmosphere-

Table 1. Details of Models Used in CMIP5 Analysis of Southern Ocean[a]

Number	Model Name	HIST	RCP45	RCP85	Vertical	Resolution at 50°S
1	bcc-csm1-1	O	O		Z	1.0 × 1.0
2	CanESM2	O		O	Z	1.41 × 0.93
3	CCSM4	O	O		Z	1.13 × 0.53
4	CNRM-CM5	O/A			Z	1.0 × 0.65
5	CSIRO-Mk3-6-0	O/A	O		Z	1.88 × 0.93
6	GFDL-ESM2G	O/A	O/A	O/A	S	1.0 × 1.0
7	GFDL-ESM2M	O/A	O	O/A	Z	1.0 × 1.0
8	GISS-E2-H	O			Z	1.0 × 1.0
9	GISS-E2-R	O/A	O	O	Z	1.25 × 1.0
10	HadCM3	O/A			Z	1.25 × 1.25
11	HadGEM2-CC	O/A	O	O	Z	1.0 × 1.0
12	HadGEM2-ES	O/A	O	O	Z	1.0 × 1.0
13	inmcm4	O	O		S	1.0 × 0.47
14	IPSL-CM5A-LR	O/A	O	O	Z	1.98 × 1.30
15	IPSL-CM5A-MR	O/A	O/A		Z	1.98 × 1.30
16	MIROC5	O/A	O/A		SZ	1.41 × 0.78
17	MIROC-ESM	O/A	O/A	O/A	SZ	1.41 × 0.93
18	MIROC-ESM-CHEM	O/A	O/A		SZ	1.41 × 0.93
19	MPI-ESM-LR	O/A	O/A	O/A	Z	1.41 × 0.89
20	MRI-CGCM3	O	O	O	Z	1.0 × 0.5
21	NorESM1-M	O		O	S	1.13 × 0.53

[a]Each column "O" means that we used the ocean component, and "A" means that we used the atmospheric component. Vertical refers to the vertical coordinate scheme, where Z indicates depth level and S sigma coordinates (SZ are hybrids). Resolution is zonal mean ocean grid longitude and latitude differences at 50°S. ESM (Earth System Model) indicates if model includes a coupled carbon cycle.

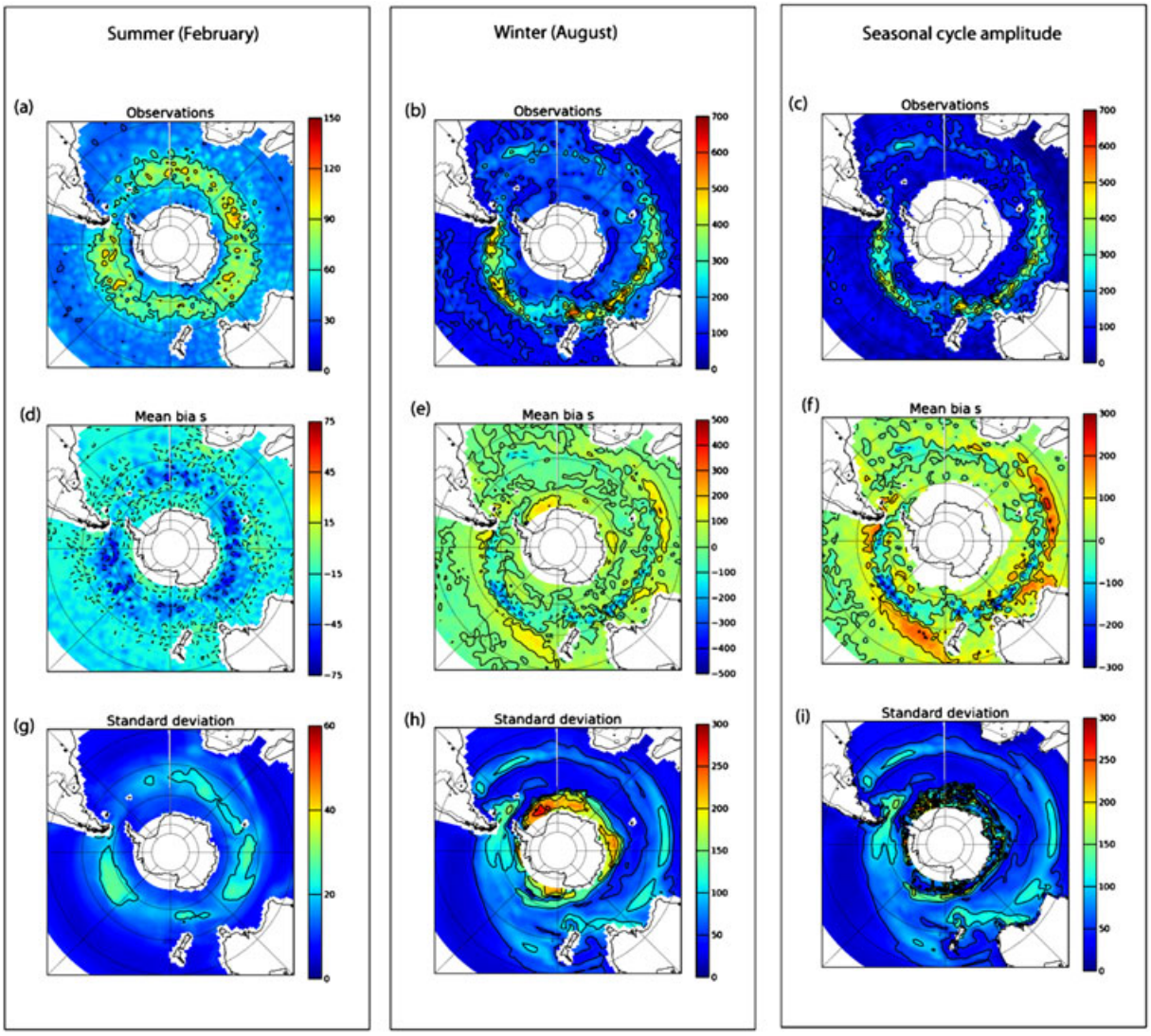

Figure 1. Multi-model representation of summer, winter and amplitude of MLD seasonal cycle (in meters; climatological mean over the "historic" period). (a–c) Observed MLD, (d–f) multi-model mean bias, (g–i) multi-model standard deviation of bias. Analysis for summer is shown on the left column (i.e., Figures 1a, 1d, and 1g), for winter on the middle column (i.e., Figures 1b, 1e, and 1h) and for the amplitude of the seasonal cycle on the right column (i.e., Figures 1c, 1f, and 1i).

ocean general circulation models (AOGCMs) and Earth system models (ESMs). The required variables were downloaded from the British Atmospheric Data Centre portal (http://badc.nerc.ac.uk/home/index.html). Variables from both the ocean and atmosphere components of the model were used (temperature, salinity, pressure, and velocity for the ocean component; heat and freshwater air-sea fluxes for the atmospheric component). At the time of writing, 21 models were available with all the required ocean parameters, while only 14 models had both atmospheric and ocean parameters available (see Table 1).

[7] The present-day mean state of the models is assessed through comparisons with observation-based estimates of the Southern Ocean mixed layer properties. Mixed-layer structure and characteristics have been computed on individual temperature/salinity profiles from the Argo program and from ship-based observations [*Sallée et al.*, 2010b]. The term "present day" is defined here as the 30 year period 1976–2005. To assess the model representation of the present state, data from the CMIP5 "historical" forcing runs is used. The historical runs are fully coupled experiments that are forced by 20th century variations of important climate drivers, including both natural and anthropogenic factors. Two future scenarios are also considered: Representative Concentration Pathway (RCP) 4.5 (a medium mitigation scenario) and RCP 8.5 (a high emissions scenario), where the numbers refer to approximate estimates of radiative forcing at the year 2100. A full range of anthropogenic forcing factors are included in the RCP scenarios (GHGs, aerosols, chemically active gases and land use) along with a repeating 11 year solar cycle (repeating solar cycle 23), which are detailed in *Meinshausen et al.* [2011]. In this paper, 21st century change is defined as the difference between the mean

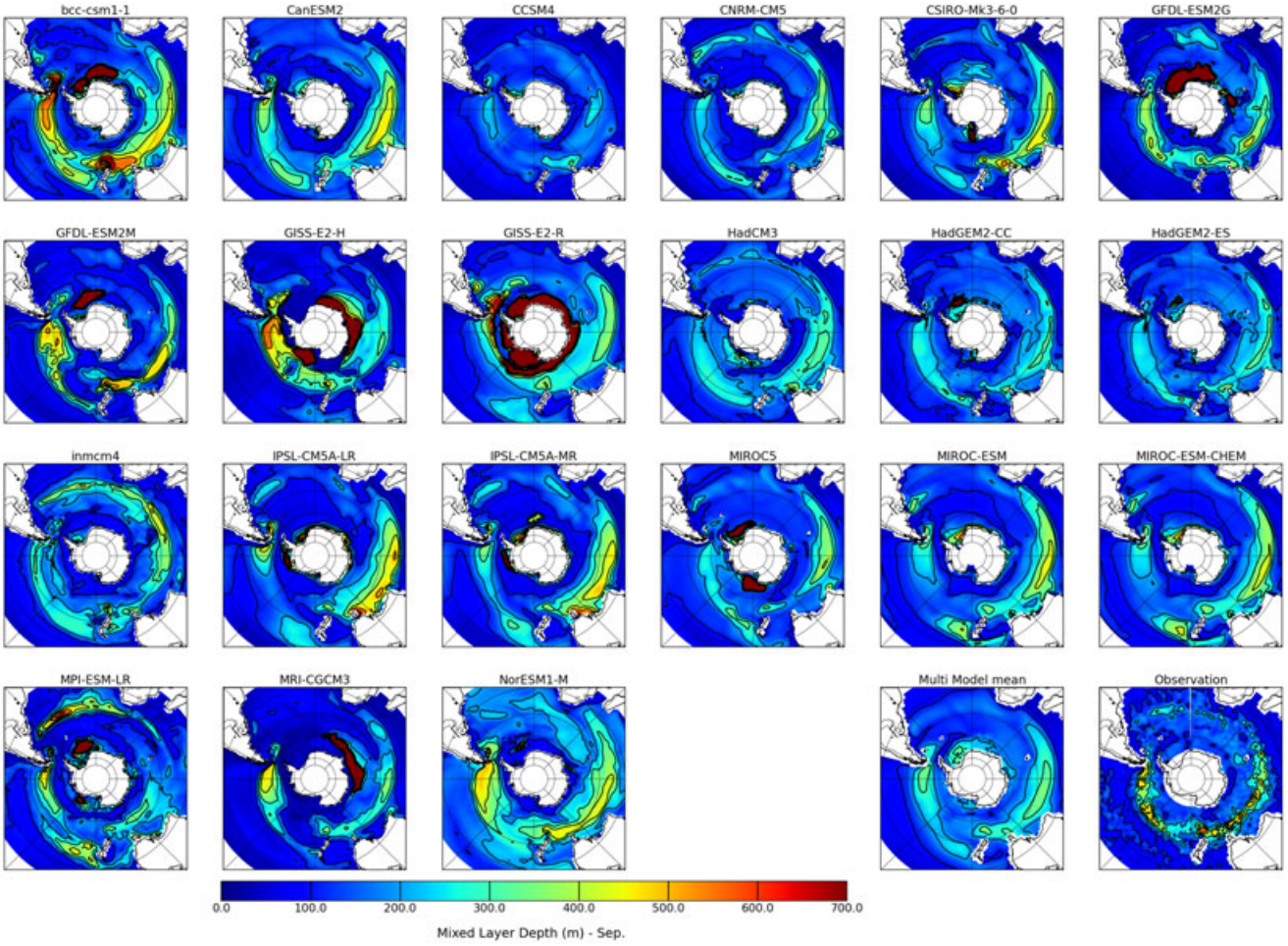

Figure 2. September mixed-layer depth (in meters) averaged over the "historic" period in each model. The multi-model mean and observation-based estimate are in the bottom right corner.

over the period 2070–2100 following either RCP8.5 or RCP4.5 minus the mean over the period 1976–2005 in the historical experiment.

2.2. Mixed-Layer Definition

[8] Mixed-layer depth (MLD), mixed-layer temperature, salinity, density, and stratification at the base of the mixed layer were computed from every monthly-mean model of temperature, salinity and pressure. All calculations were performed on the original model grid and then gridded on a regular consistent grid to ease inter-model comparisons. Thirty year monthly averages were then performed. Groups participating in CMIP5 provide MLD as one of their outputs, however, we chose to compute MLD from original temperature/salinity fields in order to make sure a consistent definition is used across all models. We calculated the MLD with a surface-density-difference criterion of $\Delta\sigma \geq 0.03$ kg m^{-3} [*Sallée et al.*, 2006; *de Boyer Montégut et al.*, 2004]. For the observation-based products, we calculated the MLD for every Southern Ocean profile with the same criterion and mapped monthly averages by a loess fitting method [*Ridgway et al.*, 2002; *Sallée et al.*, 2010b]. The extensive coverage provided by the Argo data set enabled us to obtain monthly maps of MLD on half-degree grids. Example of potential density profiles and associated mixed-layer determination are shown in Appendix A, along with a discussion of associated errors.

3. Southern Ocean Mixed Layer Representation

[9] A strong seasonal cycle in MLD exists in the Southern Ocean, exceeding more than 400 m in some locations north of the Antarctic Circumpolar Current (ACC) [*Sallée et al.*, 2010b]. Winter cooling destabilizes the water column and increases MLD such that the maximum MLDs are found in late austral winter (September) before warming during spring and early summer rapidly re-establishes the shallow summer mixed layer. As introduced above, our paper focuses mostly on the deep winter mixed-layer convection that develops on the equatorward (northern) edge of the ACC. Before tackling the analysis of winter MLD representation, we find it useful to document the ability of models to represent summer mixed layer and the amplitude of the seasonal cycle. Indeed, while the winter mixed-layer depth is crucial for the ventilation of the Southern Ocean [*McCartney*, 1977; *Hanawa and Talley*, 2001; *Sallée et al.*, 2010a], characteristics of the water subducted in winter are set all year round. In addition, summer depth is critical for ocean surface chemistry and biological activity [*Lovenduski*

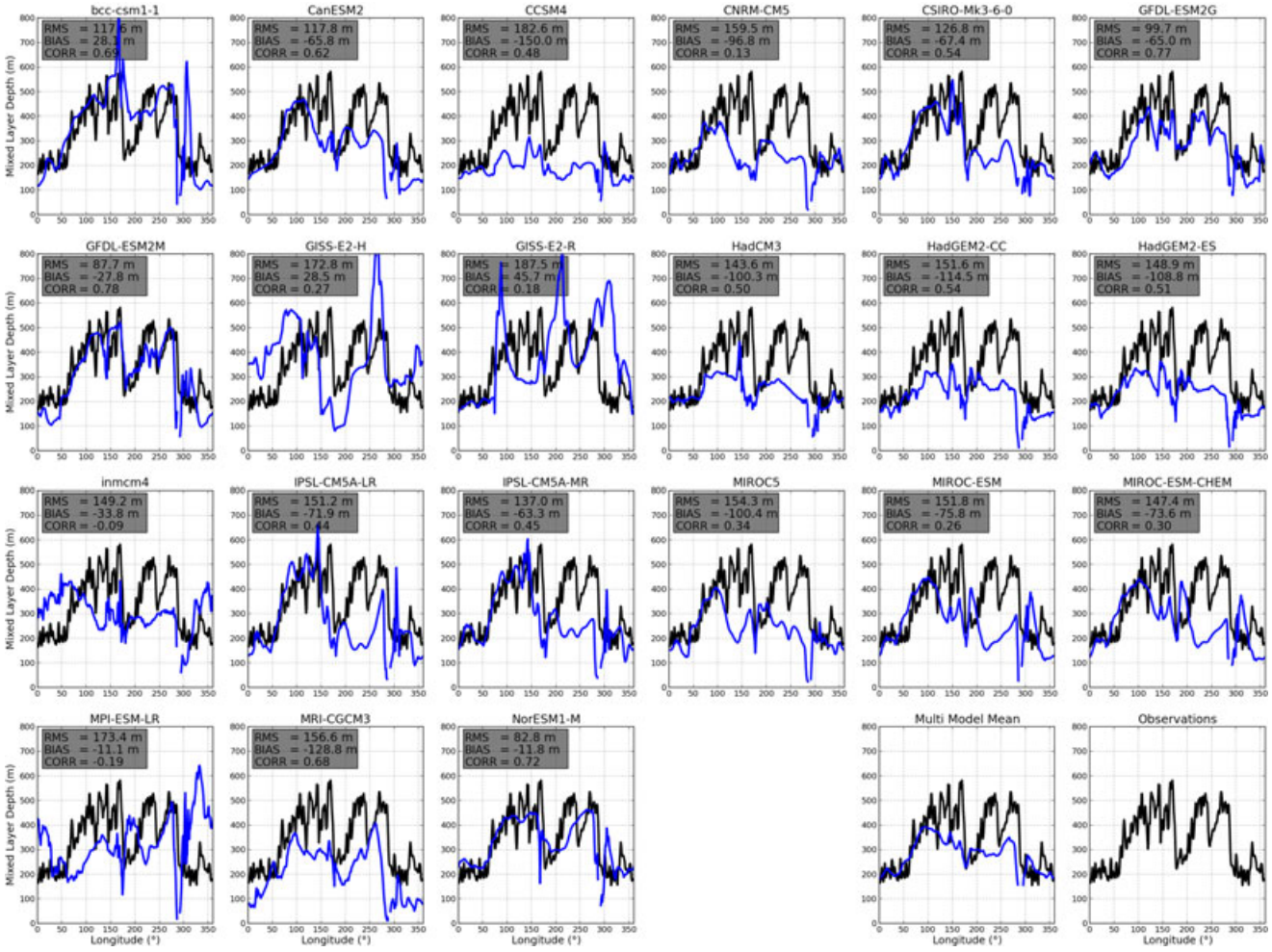

Figure 3. September mixed-layer depth (in meters) at MLD_{max} averaged over the "historic" period in each model. Multi-model mean and observation-based estimate are in the bottom right corner. In each panel, the root mean square of MLD_{max} is given (RMS), along with the mean bias between observation-based and model MLD_{max} (BIAS, negative means model shallower than observation), and the along-stream correlation between observation-based and model MLD_{max} (CORR).

and Gruber, 2005; *Sallée et al.*, 2010b], which are processes implemented in the Earth System Models participating in CMIP5.

[10] The summer (February) mixed-layer structure in the Southern Ocean is characterized by a circumpolar band of deep mixed layers reaching 60–90 m in the latitude band 50°S–60°S (Figure 1a). Outside of this band, mixed layers are shallower at around 50 m. The deep circumpolar band strongly destabilizes in winter to reach depths up to 400–700 m (Figure 1b). The band is narrower in winter and concentrated only on the equatorward edge of the ACC. This is where mode and intermediate waters are formed [*McCartney*, 1977; *Hanawa and Talley*, 2001; *Sallée et al.*, 2006, 2008a]. On average, the models tend to be biased shallow compared with observations, both in summer and winter, in the band of deepest mixed layers (Figures 1d–1e). The multi-model average of bias is significant both in winter and in summer. In summer, the multi-model average of bias reaches 50–70 m, while in winter, it reaches 100–200 m. We also find that in winter, on average, models simulate too wide a band of deep mixed layer, which extends too far equatorward, as revealed by a deep bias on the northern edge of the deepest mixed-layer band (averaged deep bias of 100–200 m; Figure 1e).

[11] The summer and winter mixed-layer depth biases translate into a misrepresentation of the mixed-layer seasonal cycle compared with observations (Figure 1f). The amplitude of MLD seasonal cycle is too small by as much as 200 m in regions of deep mixed-layer convection in the eastern Indian, mid-Pacific and easter Pacific basins. In contrast, in subtropical regions directly north of the maximum mixed layer depth sector, the amplitude of the seasonal cycle is too large compared with observations by 100–200 m on average. These significant biases have important implications for the formation of mode and intermediate water. *Sallée et al.* [2010a] have shown the importance of seasonal cycle and regional structure of the deepest Southern Ocean mixed-layer depth in the subduction of water-masses. The significant deep bias in winter mixed-layer depth and seasonal cycle amplitude in the subtropical regions (western Indian and western Pacific) suggest that too large an amount of subtropical mode water is subducted in climate models.

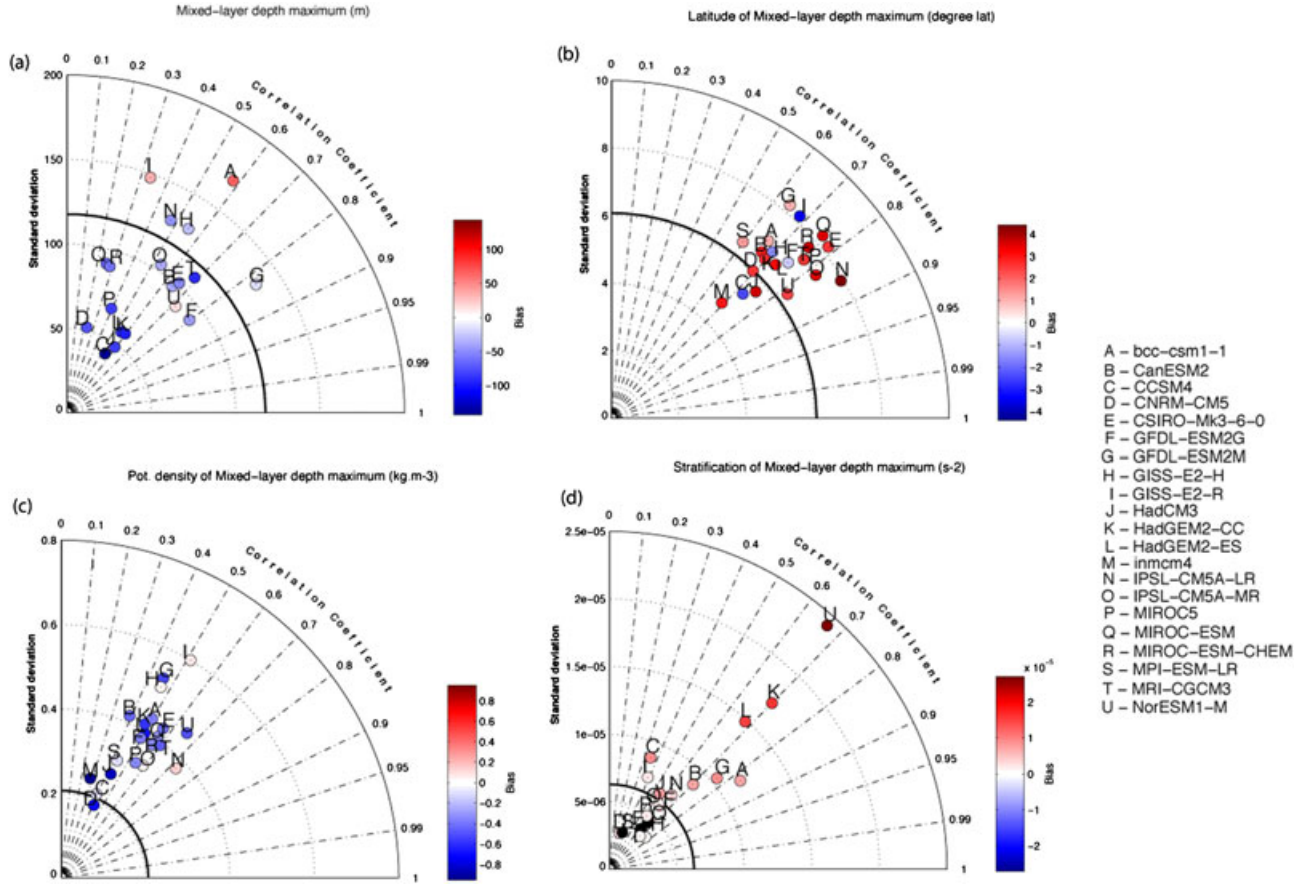

Figure 4. Taylor diagram of several key mixed-layer diagnostics along the maximum winter mixed-layer band around the circumpolar belt: (a) Depth, (b) latitude, (c) potential density, and (d) stratification. The results are calculated from each model for the "historic" time period. In each quadrant, correlation with observation-based estimate correspond to the angle; the radius is associated with the standard deviation of each variable around the circumpolar belt; standard deviation from observation-based estimate is superimposed in thick black; color indicate the mean bias compared to observations.

Consistent with this, we show in a companion paper that mode water density is biased light due to an unrealistically too large formation of subtropical mode water in the western Indian and western Pacific sectors, and a too weak formation of subantarctic mode water in the eastern Indian and Pacific sectors [*Sallée et al.*, 2013].

4. Understanding The Bias in Winter Mixed-Layer Depth

[12] The multi-model average of MLD bias described above can be used to understand the general shortcomings of the ensemble of models, however, it hides a range of very distinct structures across the models. In this section, we detail the spread of MLD patterns in each model and analyze the forcing to better understand what primarily leads to the distinct MLD representations across the models. We focus on the circumpolar band of very deep mixed layer (MLD_{max}) that develops on the northern edge of the Antarctic Circumpolar Current in winter, where mode and intermediate waters form [*McCartney*, 1977; *Hanawa and Talley*, 2001; *Sallée et al.*, 2006].

4.1. Description of the Circumpolar Structure

[13] Each of the 21 models do reproduce a deepening of the mixed layer on the equatorward edge of the ACC, implying that the basic physics responsible for deep convection is represented in the models (Figure 2). The fundamental physics are associated with (i) the presence of the ACC and the associated tilted isopycnals that create favorable conditions for the development of a deep surface layer and (ii) the intense winter buoyancy loss due to surface fluxes and Ekman transport [e.g., *Rintoul and England*, 2002; *Sallée et al.*, 2006, 2008a]. However, the circumpolar structure and the depth of winter mixed layers both vary widely across the different models (Figure 3), and we will now examine this structure basin by basin: Indian, Pacific and Atlantic.

[14] While the deep winter mixed layer band in the Indian basin is present in all models (except one: *CCSM4*), a number of models show a clear equatorward offset (*IPSL-CM5A-LR*, *IPSL-CM5A-MR*, *MIROC-ESM-CHEM*, *MIROC-ESM*; see Figure 2). Interestingly, the four models that show the clearest equatorward offset have also been shown to have a large equatorward bias (by 4°–6° latitude) in the position of their atmospheric surface westerly wind jet in the Indian sector [*Bracegirdle et al.*, 2013].

[15] Deep mixed layers in the Pacific sector often do not extend far enough westward in the models in the central basin and are positioned too close to the Drake Passage

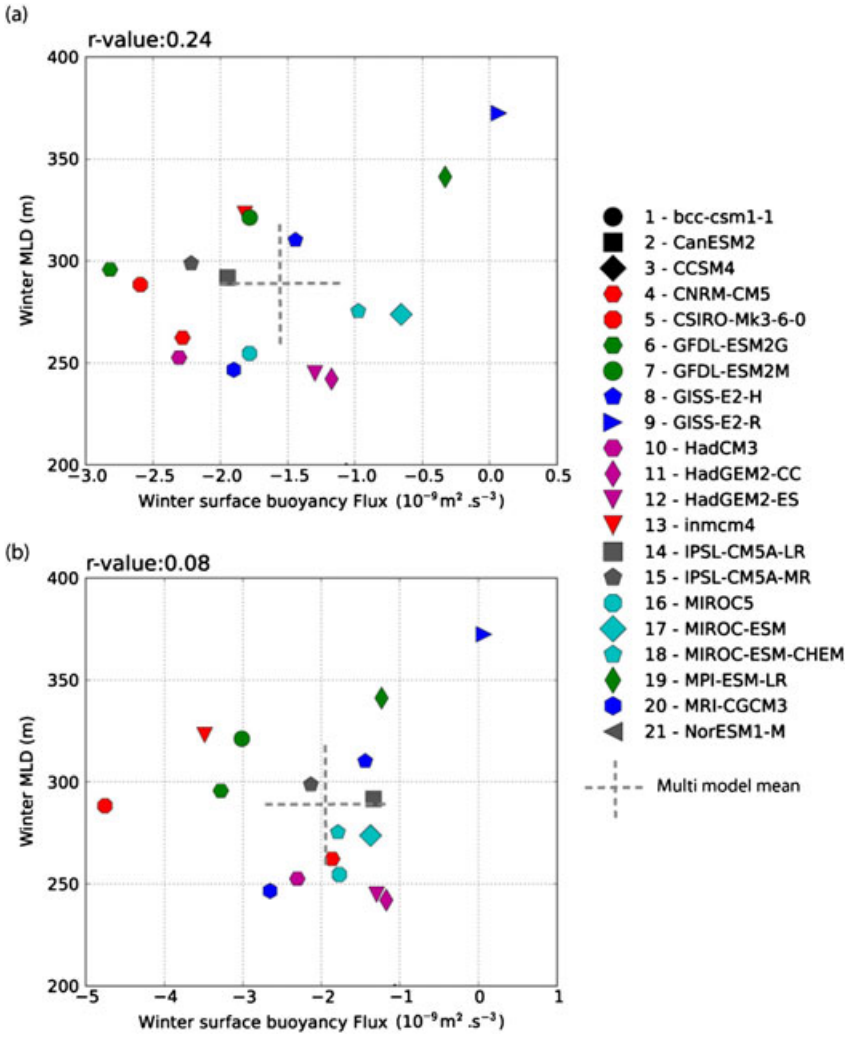

Figure 5. Mixed-layer depth versus winter buoyancy flux. Winter buoyancy fluxes and mixed-layer depth are averaged over the region MLD_{max} for each model over the "historic" period. Buoyancy fluxes include either (a) only air-sea fluxes, or (b) air-sea fluxes and Ekman fluxes. Note that in this figure, we only show models for which we had access to buoyancy flux (see Table 1).

(∼ 290°E; e.g., *IPSL-CM5A-LR, MIROC-ESM, MIROC-ESM-CHEM, HadGEM2-CC, MRI-CGCM3, CSIRO-Mk3-6-0, IPSL-CM5A-MR*; see Figures 2 and 3). Again, some of the models with the largest biases in the Pacific have been found to have strong atmospheric jet bias [*Bracegirdle et al.*, 2013]. But others have large MLD biases without being particularly biased in wind. This suggests that other processes must contribute to control the MLD and its regional structure. We investigate these below, in section 4.2.

[16] Most models re-stratify in the Atlantic sector, downstream of Drake Passage, however, there are two notable exceptions with mixed layers up to 500–700 m in the Atlantic (*inmcm4* and *MPI-ESM-LR*; see Figures 2 and 3). These two models are not particularly different from others in their representation of atmospheric jet [*Bracegirdle et al.*, 2013]. We therefore investigate alternative control factors in section 4.2.

[17] A more quantitative way to evaluate the structure of MLD_{max} in each model, is to plot Taylor diagrams of the circumpolar structure of their properties compared with observation (Figure 4). Models that best reproduce the circumpolar structure of MLD_{max} have a correlation with the observed circumpolar structure peaking at 0.8 (*GFDL-ESM2M* and *GFDL-ESM2G*). For all other models, correlations range from 0.2 to 0.7, and almost all models show a shallow bias (Figure 4a). Only three models out of the 21 models exhibit a deep bias compared with observations. In contrast, the circumpolar structure of the latitude of MLD_{max} is reproduced much more accurately by all models, with correlations with the observed structure ranging from 0.6 to 0.8 (Figure 4b). The latitude of MLD_{max} is indeed strongly constrained by the meridional excursions of the ACC that are themselves controlled by the largest topography structures of the Southern Ocean [*Moore et al.*, 1999; *Sallée et al.*, 2008b; *Meijers et al.*, 2012]. However, as suggested in Figure 2, modeled MLD_{max} are often biased equatorward compared with observational data (by 1°–3° latitude, Figure 4b). Consistent with an equatorward and shallow bias, we find that modeled potential density at MLD_{max} is lighter than observed by ∼0.2–0.8 kg m^{-3} (Figure 4c).

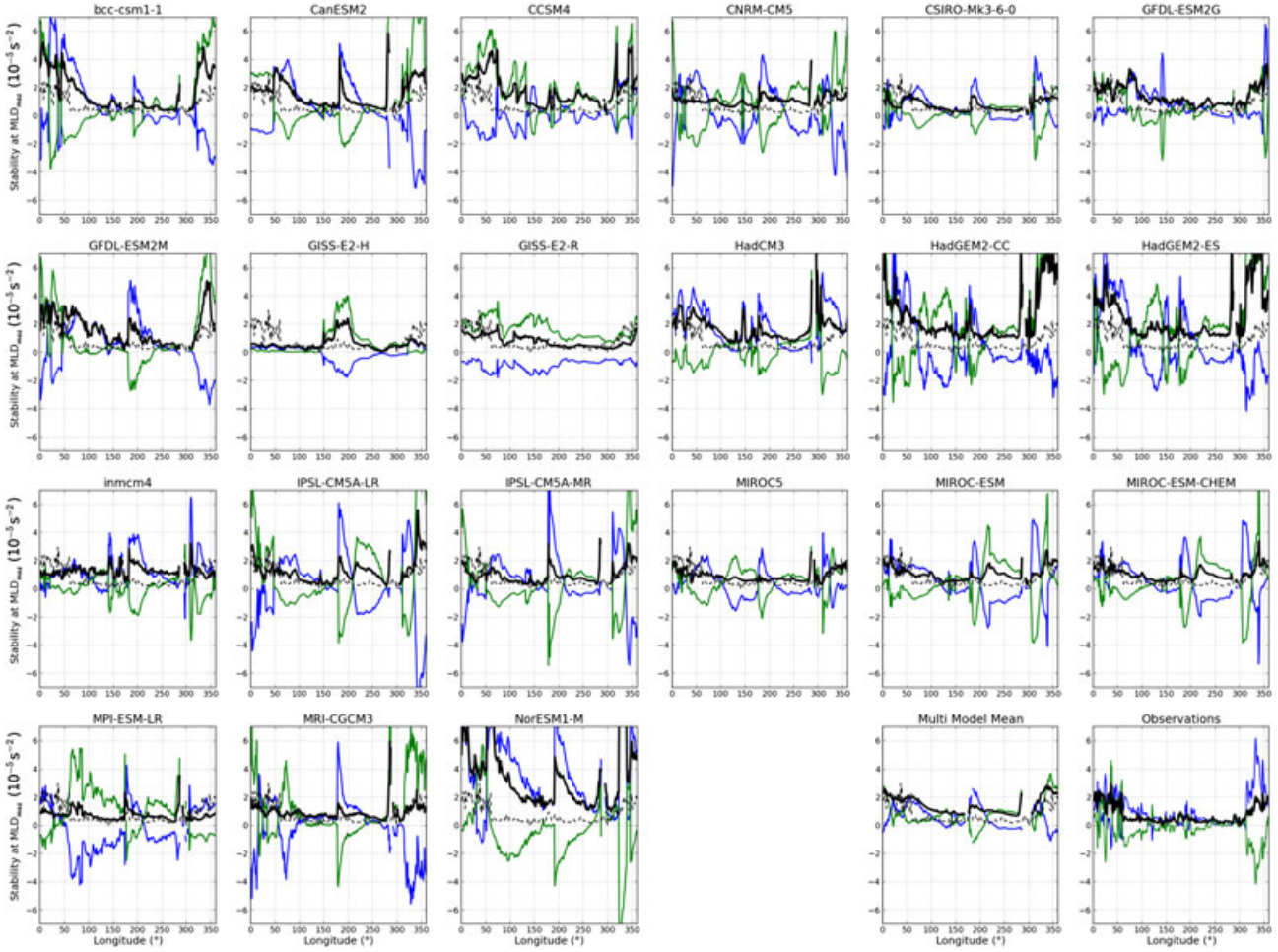

Figure 6. Stability at the base of the winter mixed layer at MLD_{max} averaged over the "historic" period in each model. (black) total, (green) haline and (blue) thermal contributions. Multi-model mean and observation-based estimate are in the bottom right corner.

4.2. Primary Forcing Controlling the Depth and Structure of Winter Mixed Layers

[18] As described above, the mixed layer creates a dynamic link between the atmospheric forcing and subsurface mode and intermediate water layers. It is therefore important to understand the causes of MLD_{max} bias as they likely skew Southern Ocean ventilation. A number of observation-based studies have analyzed the primary forcing controlling the depth of the mixed layers, and they have all consistently concluded that the two dominant forcings were winter air-sea buoyancy loss and winter Ekman buoyancy flux [e.g., *Rintoul and England*, 2002; *Sallée et al*., 2006; *Dong et al*., 2008]. We, therefore, investigate here the relationship between the modeled mixed-layer depth and the intensity of buoyancy forcing averaged over the region MLD_{max} (Figure 5). On average, over the band of MLD_{max}, the winter air-sea buoyancy loss ranges from –3 to 0×10^{-9} m^2 s^{-3}, depending on the model, with a multi-model mean of -1.55×10^{-9} m^2 s^{-3}. We note that this circumpolar mean hides large regional variations. Given the lack of accuracy of air-sea buoyancy fluxes from observation-based reanalysis in the Southern Ocean [e.g., *Liu et al*., 2011], we do not attempt a comparison with reconstructed observed buoyancy fluxes. Here, our goal is not to assess the accuracy of air-sea buoyancy flux; instead, it is to investigate whether there is a relationship between the winter MLD simulated in models and their air-sea buoyancy flux. Interestingly, although we expect that in any given model, winter buoyancy flux dominate the mixed-layer convection, we find that the multi-model spread in winter MLD is not well correlated with winter buoyancy flux (Figure 5a). We find a correlation of 0.24 between winter MLD and air-sea buoyancy fluxes in the models, which is small and in the opposite direction to that which might be anticipated on physical grounds (removing the two obvious outliers, *GISS-E2-R* and *MPI-ESM-LR*, still give a weak correlation of –0.11). Adding Ekman fluxes to the calculation of buoyancy fluxes degrades the correlation even more (correlation of 0.08; Figure 5b).

[19] We therefore conclude that some other parameters that differ between models must have a strong preconditioning forcing that dominates over winter buoyancy fluxes. Winter buoyancy fluxes act to break the stratification at the base of the mixed layer. We hypothesize that if the stratification in models is biased too strong, this stratification may be the dominant factor determining the maximum MLD. In other words, models that tend to be too stratified might struggle more to break the stratification barrier and

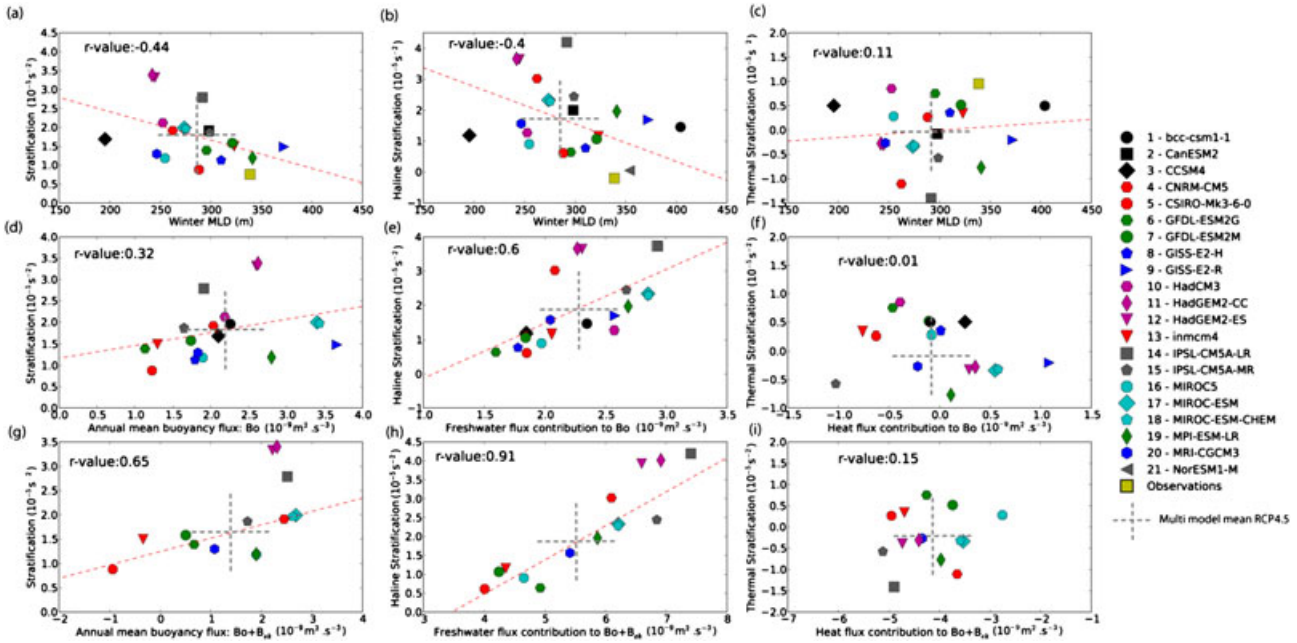

Figure 7. Analysis of the maximum September MLD, stratification at the base of the mixed layer, and surface buoyancy fluxes for the "historic" period. The upper row (a–c) presents a comparison of the mean maximum winter MLD in each model versus the spatial mean stratification at the base of these mixed layer, together with the observational values, for Figure 7a, the total stratification, Figure 7b, the haline contribution to stratification and Figure 7c, the thermal contribution to stratification. The middle row (d–f) presents a comparison of the spatial mean stratification at the base of the maximum winter mixed layer versus the annual mean air-sea flux of buoyancy: Figure 7d, total stratification versus total air-sea buoyancy flux; Figure 7e, haline stratification versus air-sea freshwater flux; Figure 7f, thermal stratification versus air-sea heat flux. The bottom row (g–i) is the same as the middle, but including annual mean Ekman buoyancy flux in addition to annual mean air-sea buoyancy flux. Note that the number of model display varies, depending on whether we had access to buoyancy flux (see Table 1).

convect deeply, even if the winter buoyancy loss is correctly represented. The stability of a water column is characterized by the Brunt-Vaïsala coefficient N defined by: $N^2 = \frac{g}{\rho}\frac{\partial \rho}{\partial z}$. The column is stable when N is positive. In support of our hypothesis, we find that all models, without exception, are biased too stratified at the base of the winter mixed layer compared with observations (Figure 4d).

[20] To explore this further, Figure 6 shows the circumpolar structure of stratification in models versus observed stratification. In regions where the deepest winter mixed layers develop (~90°E–150°E and 220°E–300°E), the observed stratification at the base of the mixed layer minimizes at around $0.1–0.2\times10^{-5}$ s^{-2}. In those regions, most models are more than twice as stratified as the observations. To better understand the cause of this large stratification bias, it is instructive to disentangle the effects of the thermocline and the halocline. The role of thermal and haline stratification on the stability at the base of the mixed layer is represented by the two terms: $N_T = -g\alpha\frac{\partial T}{\partial z}$ (thermal stability) and: $N_S = g\beta\frac{\partial S}{\partial z}$ (haline stability), where α and β are the thermal and haline contraction coefficients. In the real ocean, we find from observations that positive thermal stratification stabilizes the base of the mixed layer and is largely compensated by the haline component that tends to destabilize the water column (Figure 6; see also [*Sallée et al.*, 2006]. Observed stratification and model mean bias in thermal/haline stratification exhibit jumps in the western sectors of each basin (at 30°E–50°E, 170°E–200°E, 310°E–350°E) due to a strong meridional shift of the ACC and subtropical input of stratified water from western boundary currents. The jump downstream of Drake Passage is so intense that the base of the mixed layer stays strongly stratified all the way through the Atlantic basin, preventing deep mixed-layer formation in this sector. Note that the two models which show deep mixed layers in the Atlantic sector do not strongly re-stratify at Drake Passage (*inmcm4* and *MPI-ESM-LR*).

[21] Figure 6 indicates that there are a variety of partly compensating thermal and haline effects occurring in different regions that explain the positive stability bias. However, focusing on the models that we found above to be the most biased in terms of their MLD_{max} (i.e., *IPSL-CM5A-LR, MIROC-ESM, MIROC-ESM-CHEM, HadGEM2-CC, MRI-CGCM3, CSIRO-Mk3-6-0, IPSL-CM5A-MR*), we find that the overall positive stratification bias largely arises from a positive bias in haline stratification (fresh), partially compensated by a thermal destabilization bias. A fresh bias in the Pacific sector (170°E–300°E) is common across many models (compare with the observations; Figure 6) and arises in the multi-model mean.

[22] The importance of the stratification in controlling MLD_{max} is highlighted when evaluating the mean stratification against mean MLD_{max} in each model (Figure 7a). We

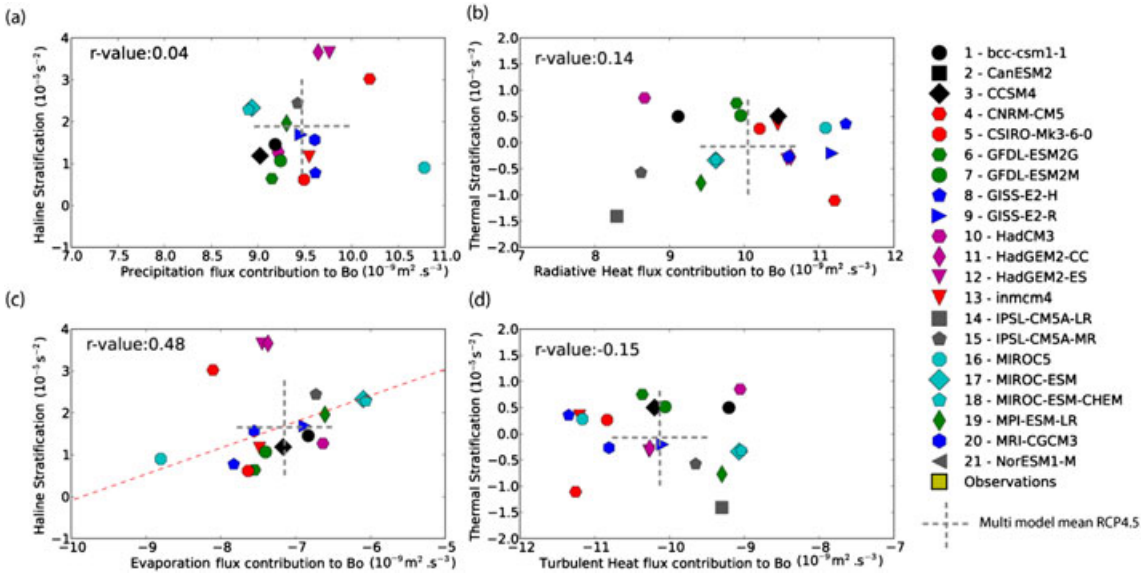

Figure 8. Contributing terms to net air-sea buoyancy flux (Bo) versus stratification at the base of the mixed layer for the historic period. (a) Precipitation and (c) evaporation flux contribution to Bo versus haline stratification; (b) radiative and (d) turbulent heat flux contribution to Bo versus thermal stratification.

find a correlation of –0.44, which implies that, as hypothesized above, the more stratified a model is, the shallower its MLD_{max}. While the correlation is just below 0.5, we find it surprisingly high given that this relationship does not take into account the intensity of winter buoyancy flux. We conclude therefore here that the intensity of winter buoyancy flux is much less crucial than the stratification to understand the spread in the ability of models to represent the deep Southern Ocean winter mixed layers. Possibly, of even greater interest is that inter-model differences in haline stratification is a much better predictor than thermal stratification (correlation of –0.4 for haline stratification versus 0.1 for thermal stratification; Figure 7b and 7c).

[23] We now investigate the causes of the haline stability bias in the models. The mean ocean stratification at the base of MLD_{max} appears weakly correlated to the annual mean

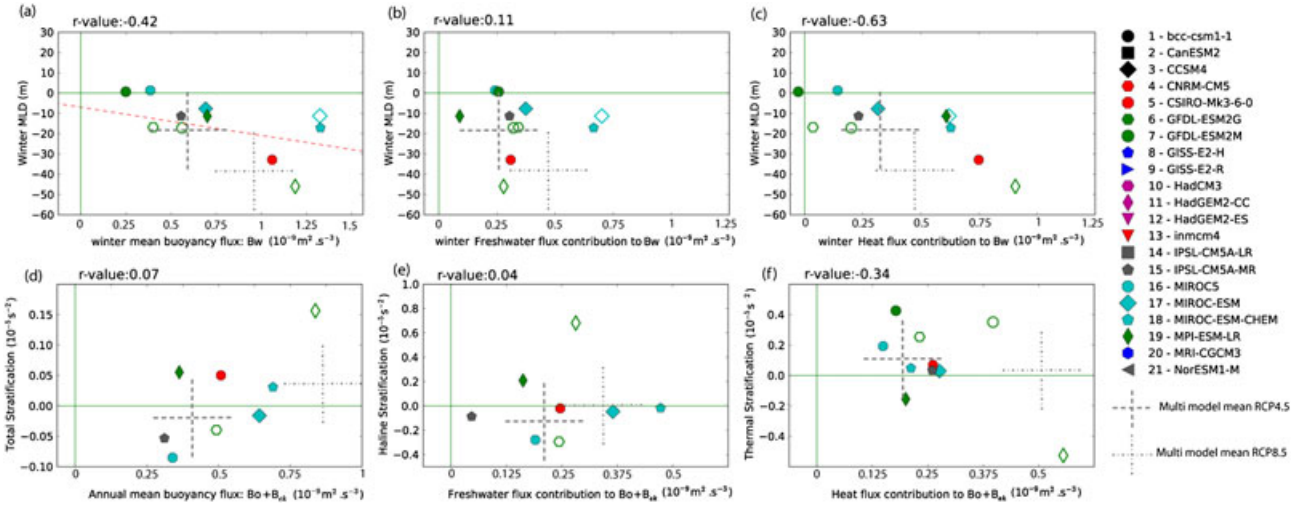

Figure 9. Maximum MLD change under future forcing scenarios and relationship with buoyancy flux and stratification changes. Circumpolar mean change of the maximum winter MLD under (filled markers) RCP4.5 and (empty markers) RCP8.5, versus (a) winter buoyancy flux change, (b) winter freshwater flux change, and (c) winter heat flux change. Change of the stratification at the base of the winter mixed layer versus buoyancy flux: Total contribution from (d) temperature and salinity, (e) from salinity only, and (f) from temperature only. Results show the change from the end of the 20th century (1976–2005) to the end of the 21st century (2070–2100). Note that the number of model display varies, depending on whether we had access to buoyancy flux for the future scenarios (see Table 1).

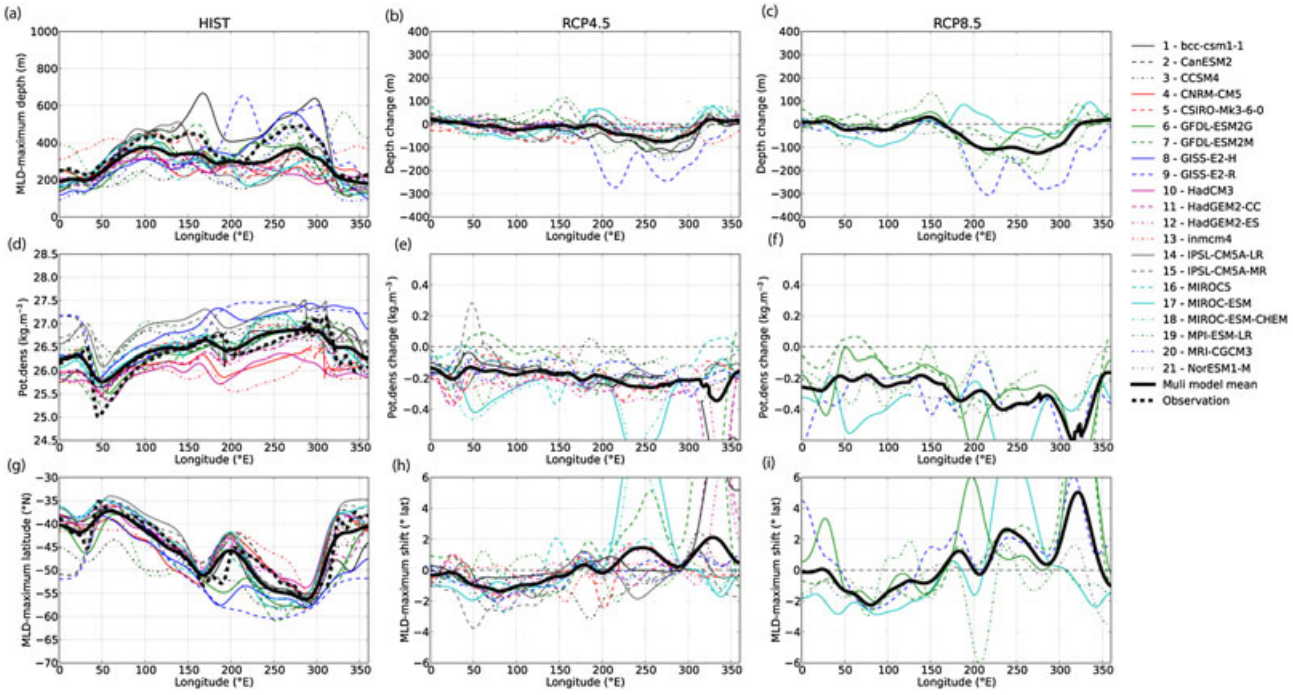

Figure 10. (left column) "Historic" (1976–2005) September mixed layer (a) depth (d) potential density and (g) latitude along the Southern Ocean circumpolar belt, following the maximum MLD at each longitude for (color) each model and (dashed black) observation. Twenty-first century change (2070–2100) under the scenario (middle column; b, e, and h) RCP4.5 and (right column; c, f, and i) RCP8.5. Note that the number of model display varies, depending on whether we had access to outputs of the future scenarios (see Table 1).

air-sea buoyancy flux input (correlation of 0.32; Figure 7d). However, when adding annual mean Ekman flux to annual mean air-sea buoyancy flux, the correlation rises to 0.65 (Figure 7g), which clearly highlights the role of buoyancy forcing (both air-sea and Ekman advection) in controlling the base of mixed-layer stratification. We remind the reader here that there could be a disconnect between annual mean buoyancy flux and stratification, as any gain or loss of buoyancy can be advected or diffused away from the mixed layer, without changing the stratification at the base of the mixed layer. In any given model, the intensity of buoyancy advection by geostrophic flow, and lateral and vertical mixing will also be key in determining the regional structure and intensity of the stratification at the base of the mixed layer [e.g., *Sallée et al*., 2006]. However, we find here that the primary drivers of the inter-model spread in stratification are the annual-mean air-sea buoyancy fluxes and the Ekman advection.

[24] Decomposing the thermal and haline contribution (both for buoyancy flux and for stratification) highlights the importance of freshwater flux. While we do not find any interesting correlation for the thermal contribution (0.01 for air-sea heat flux alone, Figure 7f, and 0.15 when adding the Ekman contribution, Figure 7i), the haline stratification is correlated at 0.6 with air-sea freshwater flux (Figure 7e), and at 0.9 when adding the Ekman contribution (Figure 7h). Because the net air-sea heat flux results from a balance of two large counter-acting fluxes, radiative and turbulent fluxes, we investigate whether a relationship between stratification and each of these individual terms could exist and cancel out in the net flux (Figures 8b–8d). However, even when looking at these individual terms, we cannot find good correlation (r = 0.14 for radiative flux and r = –0.15 for turbulent flux).

[25] Annual-mean heat flux (both Ekman and air-sea fluxes) acts to remove buoyancy in the MLD_{max} region (multi model mean of -4.1×10^{-9} m^2 s^{-3}; Figure 7i) due to large Ekman advection of cold water and a slight dominance of outgoing turbulent fluxes over incoming radiative fluxes. In contrast, freshwater fluxes act to add buoyancy, counterbalancing the loss due to heat flux and dominating over it (multi model mean of $+5.5 \times 10^{-9}$ m^2 s^{-3}; Figure 7h). Interestingly, the inter-model spread in air-sea freshwater flux primarily comes from a large spread in the evaporation flux (Figure 8c). In contrast, precipitation flux is relatively consistent across model (Figure 8a). We therefore find that the inter-model spread in stratification at the base of the mixed layer is primarily controlled by the spread in evaporation flux. Evaporation itself is mainly constrained by the net radiation flux, wind stress and the relative humidity. While beyond the scope of this study, we anticipate that, consistent with the finding of *Lorenz et al.* [2010], relative humidity is the main driver of the spread in evaporation given that we did not find good correlation between radiative flux and stratification (Figure 8b). We leave these considerations for further analysis.

[26] In summary, we find that mixed layers in the mode and intermediate water formation regions (i.e., MLD_{max}) are biased shallow and light, which mostly arises from too large freshwater inputs at the ocean surface (associated with

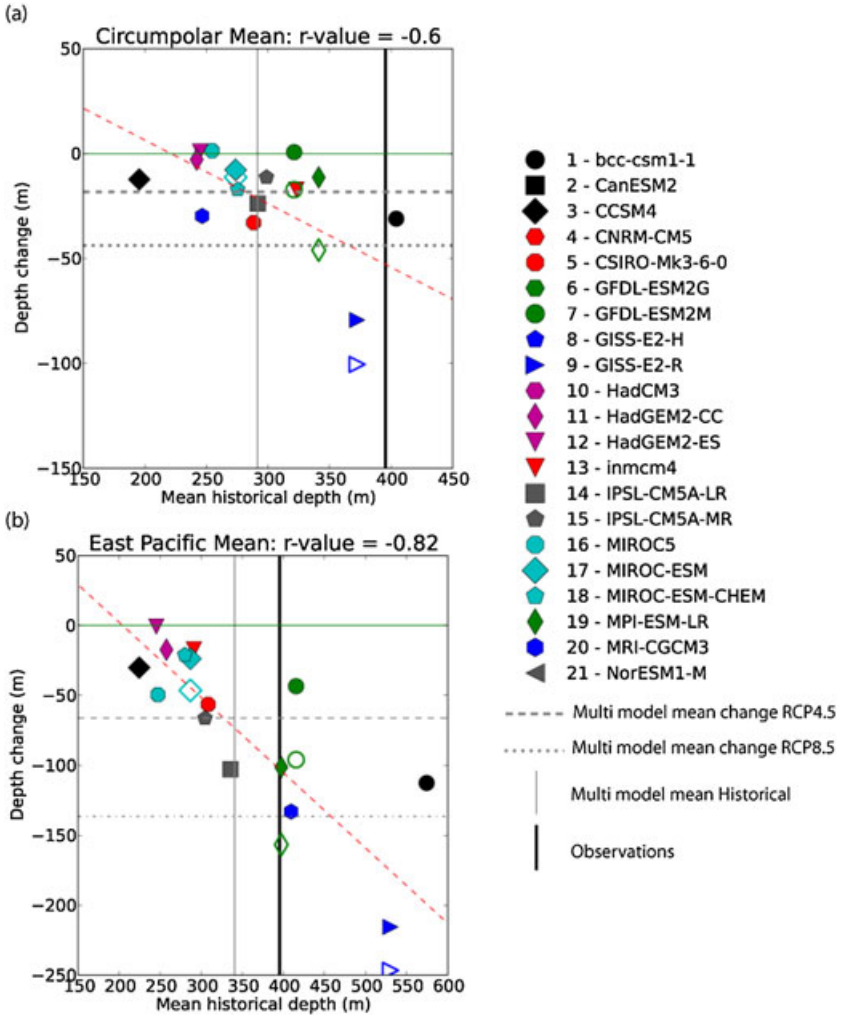

Figure 11. Future (2070–2100) mixed-layer depth change versus historical (1976–2005). (a) Circumpolar averaged value and (b) averaged on the east Pacific sector only (250°E–300°E). The results from RCP4.5 are shown as filled markers and RCP8.5 as empty markers.

air-sea fluxes and Ekman transport) that over-stratify the surface layer and prevent deep winter convection. In addition, while all forcing variable must play a signification role on stratification, we find that the large inter-model spread in the stratification at the base of the mixed layer can be explained at first order by a large spread of evaporation flux.

5. Future Changes in Southern Ocean Mixed Layer Under Increased Radiative Forcing

[27] Based on our analysis of the historical mixed layer state, we might expect that future changes in annual-mean air-sea buoyancy flux would be key to understanding future MLD changes through a shift in stratification at the base of the surface layer. However, we find that future changes of simulated annual-mean buoyancy flux (sum of Ekman and air-sea contribution) under scenario RCP4.5 and RCP8.5 are relatively small (Figure 9d; multi-model increase of 0.38×10^{-9} m^2 s^{-3} under RCP 4.5 and 0.86×10^{-9} m^2 s^{-3} under RCP8.5; a reduced number of models are shown in Figure 9 as there are fewer available models with atmospheric fluxes for the future scenarios—see Table 1) compared with historical inter-model spread values ranging from –1 to 2.9×10^{-9} m^2 s^{-3} (Figure 7g). Associated changes in stratification at the base of the mixed layer are not consistent between models (correlation of 0.07). Decomposing the haline and thermal fluxes does not improve this relationship (Figures 9e–9f).

[28] All analyzed models simulate a freshening and a warming flux (i.e., gain of buoyancy) into the MLD_{max} region under increased radiative forcing, with greater changes for the stronger forcing scenario (RCP4.5: 0.23×10^{-9} m^2 s^{-3} associated with annual-mean freshwater increase, and 0.19×10^{-9} m^2 s^{-3} associated with annual-mean heat flux increase; RCP8.5: 0.35×10^{-9} m^2 s^{-3} associated with annual-mean freshwater increase, and 0.5×10^{-9} m^2 s^{-3} associated with annual-mean heat flux increase). While it might seem surprising that some models simulate both increased buoyancy fluxes and reduced stratification, we remind the reader that the stratification we consider here is taken at the base of the mixed layer and, therefore, there is no direct relationship expected between changes in stratification and changes in buoyancy fluxes. For instance, there could be a reduction of the stratification without any fluxes

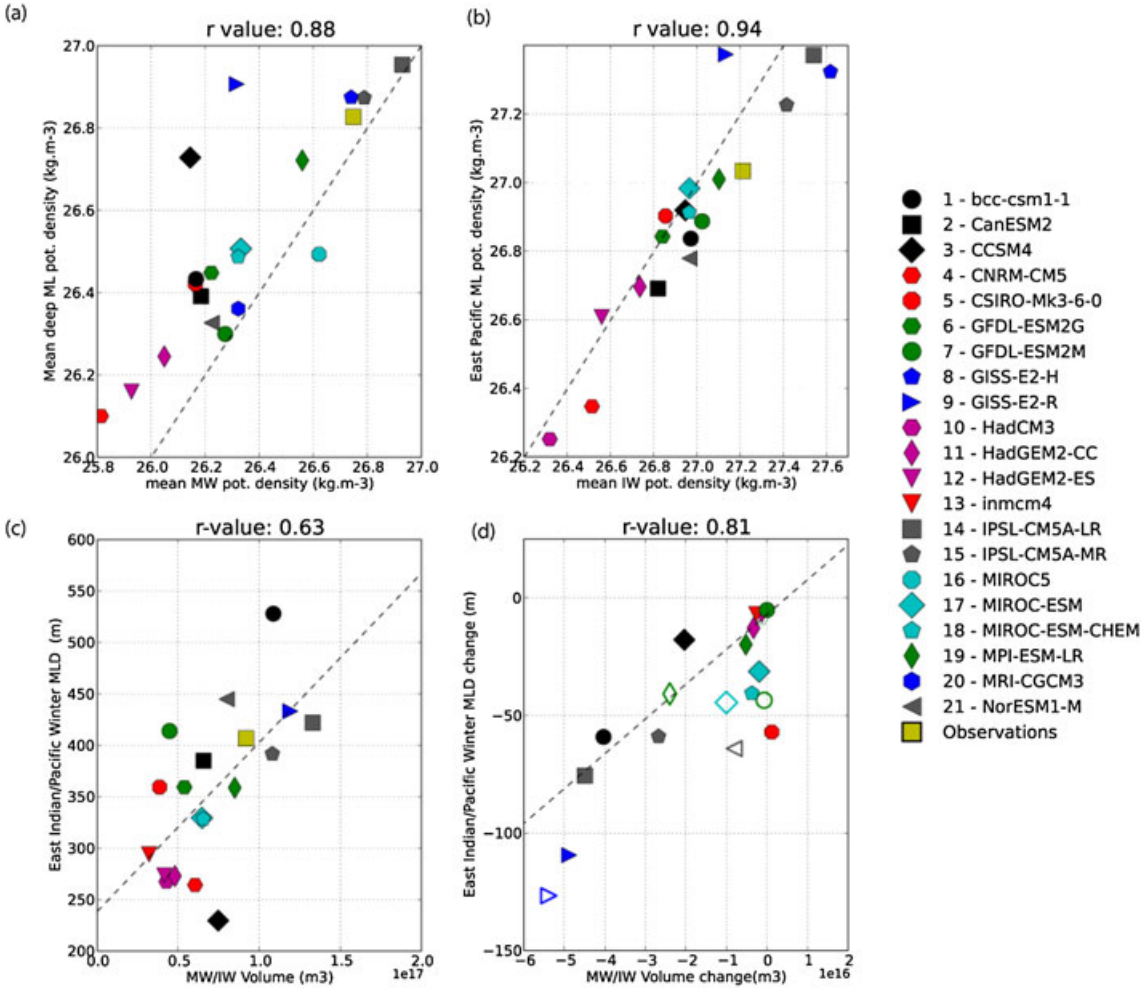

Figure 12. Relationship between winter mixed layer depth maximum and underlying mode and intermediate characteristics. (a) Mean mixed layer potential density at MLD_{max} versus underlying mode water potential density in the historical period (1976–2005). (b) Mean mixed layer potential density at MLD_{max} in the eastern Pacific basin (250°E–300°E) versus underlying Intermediate Water potential density in the historical period (1976–2005). (bottom row) Mixed layer depth at MLD_{max} in the eastern Pacific basin (250°E–300°E) versus volume of mode and intermediate water: (c) historical mean, and (d) change under RCP4.5, and RCP8.5 scenarios (2070–2100). Filled markers denote value corresponding to RCP4.5 scenario, while empty marker denote values for RCP8.5 scenario.

changes, through a shallowing of the mixed layer alone. In the assessment of the present day state presented in section 3, the relationship was less complex as we were not looking at changes in stratification but simply at the inter-model spread.

[29] Due to the small stratification changes produced (multi-model mean of -0.02×10^{-5} s^{-2} under RCP4.5 and 0.04×10^{-5} s^{-2} under RCP8.5; Figure 9d), other MLD drivers, such as winter buoyancy flux change, must be considered to explain the simulated future changes in MLD_{max}. The magnitude of winter buoyancy flux changes appears to explain most of the modeled 21st century changes of MLD_{max} (correlation of –0.42; see Figure 9a). The models simulate a circumpolar mean change of MLD_{max} up to 30 m for RCP4.5 (multi-model mean of 20 m) and up to 100 m for RCP8.5 (multi-model mean of 40 m) (see Figures 9a and 11a). These changes are explained by reduced winter buoyancy loss both in freshwater and heat flux (Figures 9b–9c). The correlation with buoyancy flux increase associated with heat flux ($r = -0.63$; Figure 9c) shows very clearly the importance of the simulated future change in heat flux for controlling the changes of mixed-layer depth in the future scenarios.

[30] The future circumpolar mean changes in MLD_{max} hide an interesting and consistent circumpolar structure. While MLD_{max} change in the Indian sector (~30°E–170°E) is relatively small, almost all models show larger shallowing in the Pacific basin (~170°E–300°E) under both RCP4.5 and RCP8.5 (Figures 10a–10c). This is consistent with larger heat flux in the Pacific basin under RCP4.5 and RCP8.5 changes (not shown). In contrast, there is a consistent lightening in potential density all along the circumpolar belt, by approximately 0.1–0.3 kg m^{-3} under RCP4.5 and 0.2–0.5 kg m^{-3} under RCP8.5 (Figures 10e–10f). The latitude of MLD_{max} exhibits a strong basin-scale variability, with a poleward shift over the Indian basin and an

equatorward shift in the Pacific basin (Figures 10g–10i). Under RCP4.5, MLD_{max} shifts by about 1° latitude (either equatorward or poleward), which increases to 2° latitude under RCP8.5. This basin scale asymmetry is explained by asymmetry in the meridional shift of the ACC described in a companion paper [*Meijers et al.*, 2012].

[31] Future changes in the depth of the mixed layer appear strongly linked to the modelled historical depth (compare across panels of Figures 10a–10c and Figure 11a). Models with the shallowest historical depth show the smallest change while models with deep historical mixed layer show larger shallowing (Figure 11a). For instance, *CCSM4* has a circumpolar mean historical depth of about 200 m and a change under RCP4.5 of 20 m or so, while *GISS-E2-R* has a circumpolar mean historical depth of about 370 m and a change under RCP4.5 around 80 m. We find a correlation of 0.6 between historical state depth and future change. As seen on Figures 10b–10c, future changes in MLD are strongly regional and mostly arise in East Pacific. When restricting the analysis of the historical state and future change to the East Pacific, the correlation increases to 0.82 (Figure 11b). Thus those models with a strong historical shallow bias in MLD in the East Pacific show little future change, whereas those which are closer to observations indicate a future shallowing of MLD in the East Pacific about 50–150 m under RCP4.5 (Figure 11b, filled markers) with greater shallowing under RCP8.5 (Figure 11b, open markers).

6. Implications for Southern Ocean Ventilation

[32] In this section, we compare the characteristics of MLD_{max} to the underlying mode and intermediate water layers that ventilate the Southern Hemisphere ocean thermocline [e.g., *Talley*, 1999]. We define mode and intermediate water based on their PV and salinity characteristics and point the reader toward our companion paper for a detailed presentation of the water-mass definition that we apply to the CMIP5 models output [*Sallée et al.*, 2013].

[33] In agreement with Stommel's mixed-layer "demon" [*Stommel*, 1979], the characteristics of winter MLD_{max} are tightly linked to the characteristics of mode water (correlation of 0.88; Figure 12a). MLD_{max} appears, however, slightly denser than the underlying mode water, by a multi-model mean offset of 0.08 $kg.m^{-3}$. This discrepancy reflects the fact that the modeled deep winter mixed-layer pools associated with mode water subduction typically extend too far equatorward in the subtropical gyre. Consistent with this, as discussed above, Figure 1 clearly shows that modeled mixed layers tend to have a too intense seasonal cycle in the subtropical regions, which would be associated with an excess subduction of light subtropical mode water. Indeed, in agreement with *Sloyan and Kamenkovich* [2007] who analyzed the CMIP3 models, we present results in a companion paper [*Sallée et al.*, 2013] that indicate most CMIP5 models subduct mode water at clearly too light densities in the western part of the basins, which densifies very quickly as it shifts into the eastern part of the basins. In contrast to the wide region over which mode waters are subducted, MLD_{max} is the circumpolar contour following the maximum mixed layer. Therefore, the density associated to MLD_{max} is expected to be larger than the density given by an average over the wide pool of deep winter mixed layers that extend in subtropical regions.

[34] Intermediate water is formed in the southeastern Pacific, directly west and within the Drake Passage (290°E), from where it spreads to the entire Southern Hemisphere and to the tropics at all longitudes [*Talley*, 1999; *Sallée et al.*, 2010a]. The subduction mechanism is very localized and strongly controlled by the ACC flowing across the sharp shallowing of MLD_{max} at the Drake Passage, which pushes water-masses laterally across the base of the mixed layer [*Sallée et al.*, 2010a]. Most models do accurately reproduce the sharp mixed-layer shallowing at the Drake Passage. Consistent with this, intermediate water potential density characteristics accord very well with eastern Pacific MLD_{max} properties (correlation of 0.94; Figure 12b).

[35] The overall volume of subducted water (mode and intermediate) also agrees well with the depth of MLD_{max} in the eastern Indian and Pacific, where these water-masses have been shown to subduct most strongly [correlation of 0.63; Figure 12c; *Sallée et al.*, 2010a]. The relationship for future change is even stronger, with a correlation of 0.81 (Figure 12d): future change in MLD_{max} in the eastern Indian and Pacific is a very good proxy for future changes in the volume of ventilated water. All models predict an overall reduction of subducted water volume associated with a shallowing of MLD_{max} under RCP4.5 and RCP8.5.

7. Conclusions and Discussion

[36] The representation of the Southern Ocean winter mixed layer has been evaluated in 21 climate models participating in the CMIP5 exercise. In the analyzed climate models, the region MLD_{max}, where mode and intermediate waters are formed and pre-conditioned, is shallower, lighter and more equatorward than observed. These results have important implications for characteristics of mode and intermediate waters and rate by which they enter into the interior ocean. This is of primary importance for the dissolution and sequestration of carbon dioxide in the interior ocean [*Séférian et al.*, 2012; *Sallée et al.*, 2012].

[37] While Southern Ocean MLD bias in climate model has been documented in the past [e.g., *Downes et al.*, 2009], in this paper, we have unraveled for the first time the primary drivers of the bias that need to be looked at if we are to improve the representation of deep Southern Ocean MLD in climate models. We identified that freshwater fluxes artificially increase the stratification of MLD_{max}, which biases the depth and density of the surface layer by preventing deep mixed layer convection. Note that we are not arguing that thermal stratification or winter buoyancy flux have no impact on MLD_{max}, but we identified the annual-mean freshwater flux as the primary source of error. Observational uncertainty and technical difficulties in obtaining good estimates of annual-mean buoyancy flux in the Southern Ocean have long been identified as one of the largest shortcomings in our knowledge of the Southern Ocean [e.g., *Liu et al.*, 2011]. However our analysis offers a fresh perspective for modelling teams to adjust their Southern Ocean fluxes to best represent the well-observed amount of haline stratification at the base of the mixed layer.

[38] Under increased radiative forcing scenarios, CMIP5 models simulate a shallowing, a lightening and a meridional

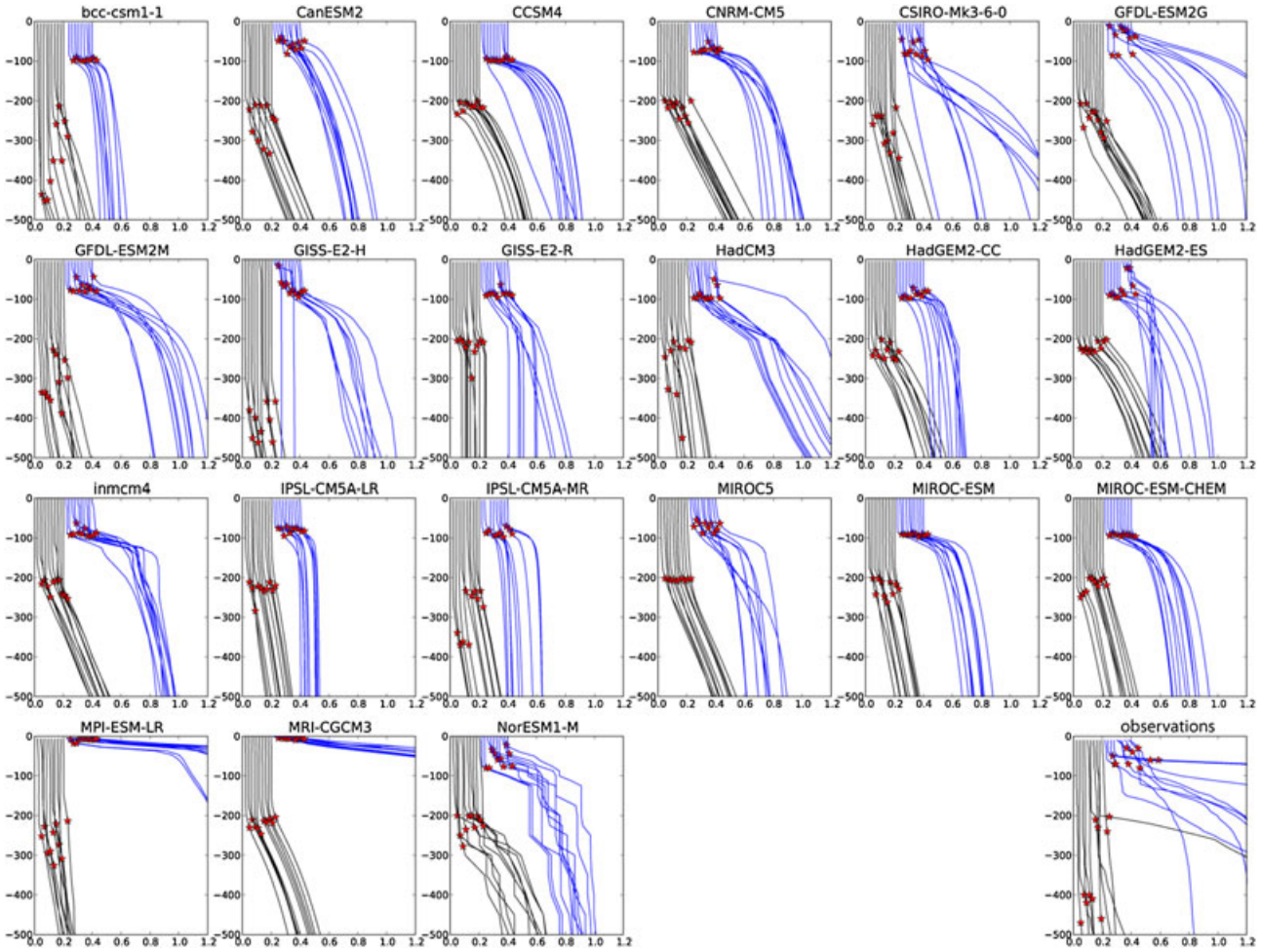

Figure A1. Twenty potential density profiles (kg m^{-3}) randomly picked in the southeastern Pacific sector (220°E–290°E) are shown for each model. For ease of reading, potential density profile minus their surface value are shown, and each profile is shifted by 0.01 kg m^{-3} compared to the previous one. For each model, 10 profiles are picked in the deep mixed-layer region (deeper than 200 m; black), and 10 profiles in shallow mixed-layer region (less than 150 m; blue). The detected mixed-layer depth is superimposed with a red star. Argo profiles randomly selected in the same way as for models, are shown in the bottom right corner.

shift of MLD_{max}. The meridional shift is equatorward in the Pacific sector and poleward in the Indian sector, and is associated with shift in ACC position [*Meijers et al.*, 2012]. The shallowing is strongly linked to increased winter heat fluxes and mostly occurs in the Pacific region. Interestingly, we found a strong state dependency between historical and future change in MLD: those models with the strongest historical bias in MLD indicate little future change, whereas those whose present-day MLD is closer to observations indicate significant shallowing of the MLD under future forcing scenarios. Importantly, given that most models are biased shallow, this suggests that future changes in MLD might be larger than most models indicate. Mixed-layer properties are tightly linked to the volume and properties of ventilated layers in the ocean interior, both in historical runs and for future changes. The state dependency in mixed layer could therefore potentially indicate that most model simulate a too weak reduction of the volume of ventilated layer. This would have large implications for sequestration of heat, freshwater, and gases such as oxygen and carbon, and could indicate that this potential climate change feedback may be underestimated by the current generation of models.

Appendix A: Definition of the Mixed Layer Depth

[39] In this study, mixed-layer depths are computed from monthly-mean fields of temperature and salinity using a surface-density difference criteria $\Delta\sigma \geq 0.03$ [*Sallée et al.*, 2006]. We made the choice to not use the CMIP5 mixed-layer depth variable because (i) it is not available for all models, (ii) there are risks that different modelling groups use slightly different definition, and (iii) we believe that the definition $\Delta\sigma \geq 0.03$ is more appropriate for the Southern Ocean [*Sallée et al.*, 2006].

[40] Figure A1 shows a series of 20 potential density profiles randomly picked in both deep and shallow mixed layer regions in the southeastern Pacific (220°E–290°E) for each model and from Argo profiles. Because profiles are

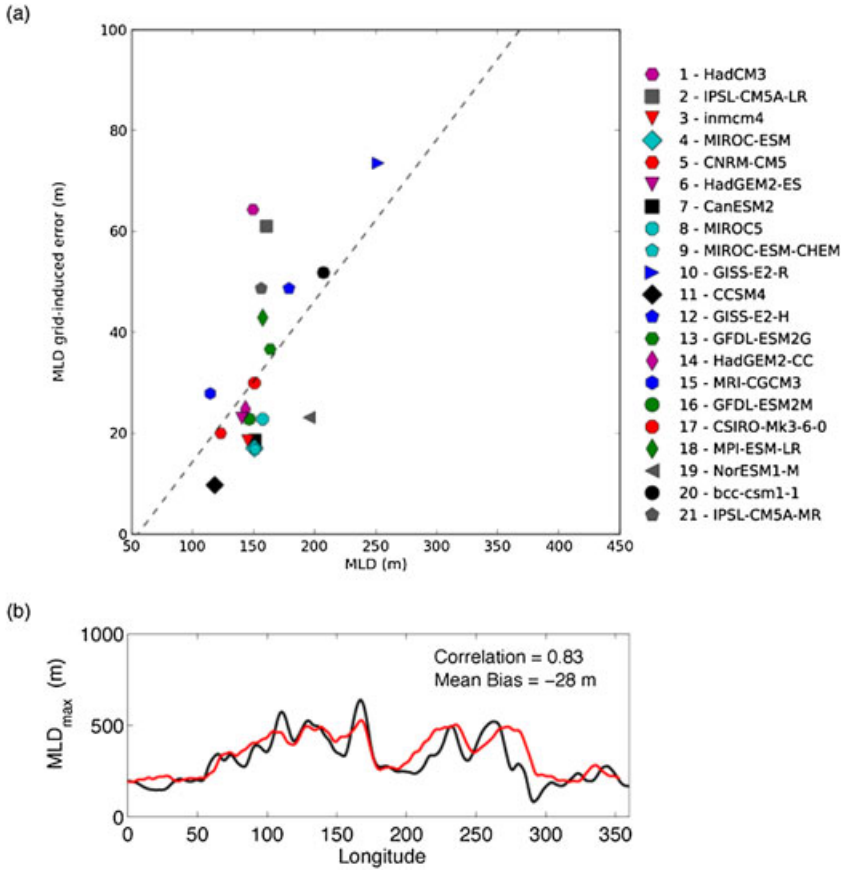

Figure A2. (a) Thirty year mean grid-induced error (m) averaged at MLD_{max} versus MLD_{max} (m). Black dotted line show the best linear fit. (b) MLD_{max} as a function of longitude deduced from (red) instantaneous Argo profile product, and (black) monthly objective analysis of available observation (EN3 product).

randomly picked in different dynamical regions for different models, the goal here is not to present inter-model differences in stratification (see main text and Figures 2 and 6 for inter-model differences). In contrast, here, we want to illustrate the accuracy of the mixed-layer detection algorithm compared to the MLD that one would have picked "by eye". As shown in Figure A1, the determined MLD is found relatively accurately at the permanent thermocline. For very deep mixed layer, the permanent thermocline is in some profiles very weak, and the picked mixed layer might be questionable. However, in the very weakly stratified region, any MLD detection algorithm would be questionable.

[41] Besides the MLD detection algorithm itself, additional issues associated with time or vertical resolution of the models, could be problematic when comparing model-derived MLD and observation-based MLD. First, the coarse vertical grid of models can create errors in the determination of MLD. Second, the monthly time-resolution of model outputs would tend to smooth out the profiles compared to instantaneous Argo profiles. We investigate these two sources of errors in turn.

[42] The effect of the vertical grid has on the detection of MLD can be easily quantified by recording the vertical depth step of the grid at the level where we compute the mixed layer. Vertical grid vary depending on the model, but they are consistently designed with increased resolution near the ocean surface. Therefore, the deeper the mixed layer, the larger the error. Figure A2a shows the model-mean grid-induced error versus mixed-layer depth. All models follow sensibly a common relationship of 10%–30% error, with maximum mean error of 75 m for *GISS-E2-R*. This error is smaller than the inter-model spread in the mixed layer described in the present paper. In addition, we tend to slightly reduce the actual grid-induced error (compared to what is shown in Figure A2a) by linearly interpolating in depth between two grid points when $\Delta\sigma \geq 0.03$ happens to fall between grid points.

[43] The impact of the time resolution of model output is hard to estimate given that we do not have access to higher time resolution of the outputs. Instead, we used monthly binned observed profile, and then derive MLD and climatological winter MLD. For this we used the UK Met-Office EN3 product, which includes monthly objective analyses of available temperature and salinity data (http://www.metoffice.gov.uk/hadobs/en3/). As expected, profiles are smoothed out by the monthly objective analysis and therefore mixed layers are found slightly shallower than from the instantaneous profile data set. We found however, very consistent structure of MLD_{max} (correlation of 0.83), with a small mean bias of 28 m compared to product derived

from instantaneous Argo profiles (Figure A2b). We expect that the bias found here is small enough to reliably compare instantaneous Argo profiles product with model MLD. EN3 objective analysis is restored to climatological value when no data is available, and climatology are poorly constraint in the Southern Ocean, so in the present study, we made the choice to use the product based on instantaneous Argo profiles only rather than the EN3 reanalysis. We note that, although the difference between EN3-derived MLD and Argo-derived MLD is overall small, it peaks locally at 50–100 m in the western (200°E–220°E) and eastern (270°E–290°E) Pacific basin. These peaks in the difference are primarily due to the fact that EN3 has a smaller area of deep ML (extending less than Argo in the western and eastern Pacific). Given that both EN3 and Argo-derived MLD have peaks at similar values in the Pacific, we believe that this difference is due to the objective analysis of EN3 including climatological value rather than due to the monthly smoothing of T/S profiles.

[44] **Acknowledgments.** Discussions with Tilla Roy on an earlier version of this study have been very valuable and constructive, and have greatly improved this work. This study is part of the British Antarctic Survey Polar Science for Planet Earth Programme. It was funded by The UK Natural Environment Research Council (grant reference number NE/J005339/1). We acknowledge the World Climate Research Programme's Working Group on Coupled Modelling, which is responsible for CMIP, and we thank the climate modeling groups (listed in Table 1 of this paper) for producing and making available their model output. For CMIP the U.S. Department of Energy's Program for Climate Model Diagnosis and Intercomparison provides coordinating support and led the development of software infrastructure in partnership with the Global Organization for Earth System Science Portals. Z.W. is supported by China National Natural Science Foundation (NSFC) Project (41276200), by the Special Program for China Meteorology Trade (Grant GYHY201306020), by Chinese National Key Basic Research Program (2010CB950301), and by a project funded by the Priority Academic Program Development of Jiangsu Higher Education Institutions (PAPD). Finally, we thank the British Atmospheric Data Centre for downloading and managing the model output data and making them available to us.

References

Anderson, R. F., S. Ali, L. I. Bradtmiller, S. H. H. Nielsen, M. Q. Fleisher, B. E. Anderson, and L. H. Burckle (2009), Wind-driven upwelling in the Southern Ocean and the deglacial rise in atmospheric CO2, *Science*, *323* (5920), 1443–1448.

Axell, L. (2002), Wind-driven internal waves and Langmuir circulations in a numerical ocean model of the southern Baltic Sea, *J. Geophys. Res*, *107* (C11), 3204.

Bracegirdle, T. J., E. Shuckburgh, J. B. Sallée, Z. Wang, A. J. S. Meijers, N. Bruneau, T. Phillips, and L. Wilcox (2013), Assessment of surface winds over the Atlantic, Indian and Pacific Ocean sectors of the Southern Ocean in CMIP5 models: Historical bias, forcing response, and state dependence, *J. Geophys. Res.*, *118*(2), 547–562, doi:10.1002/jgrd.50153.

Burchard, H., and H. Rennau (2008), Comparative quantification of physically and numerically induced mixing in ocean models, *Ocean Model.*, *20*, 293–311.

Danabasoglu, G., S. C. Bates, B. P. Briegleb, S. R. Jayne, M. Jochum, W. G. Large, S. Peacock, and S. G. Yeager (2012), The CCSM4 ocean component, *J. Climate*, *25*(5), 1361–1389.

de Boyer Montégut, C., G. Madec, A. S. Fischer, A. Lazar, and D. Iudicone (2004), Mixed layer depth over the global ocean: An examination of profile data and a profile-based climatology, *J. Geophys. Res.*, *109*, C12003, doi:10.1029/2004JC002378.

Dong, S., J. Sprintall, S. T. Gille, and L. Talley (2008), Southern Ocean mixed-layer depth from Argo float profiles, *J. Geophys. Res.*, *113*(C6), C06013, doi:10.1029/2006JC004051.

Downes, S. M., N. L. Bindoff, and S. R. Rintoul (2009), Impact of climate change on the subduction of mode and intermediate water masses in the Southern Ocean, *J. Climate*, *22*, 3289–3302.

Downes, S. M., N. L. Bindoff, and S. R. Rintoul (2010), Changes in the subduction of Southern Ocean water masses at the end of the 21st century in eight IPCC models, *J. Climate*, *23*, 6526–6541.

Fox-Kemper, B., R. Ferrari, and R. Hallberg (2008), Parameterization of mixed layer eddies. Part I: Theory and diagnosis, *J. Phys. Ocean.*, *38*, 1145–1165.

Fox-Kemper, B., G. Danabasoglu, R. Ferrari, S. M. Griffies, R. W. Hallberg, M. M. Holland, M. E. Maltrud, S. Peacock, and B. L. Samuels (2011), Parameterization of mixed layer eddies. III: Implementation and impact in global ocean climate simulations, *Ocean Model.*, *1-2*, 61–78.

Hanawa, K., and L. D. Talley (2001), Mode waters, in *Ocean Circulation and Climate*, edited by G. Siedler, J. Church, and J. Gould, pp. 373–386, Acadamic Press, San Diego, Calif.

Ito, T., M. Woloszyn, and M. Mazloff (2010), Anthropogenic carbon dioxide transport in the Southern Ocean driven by Ekman flow, *Nature*, *463* (7277), 80–83.

Lee, M. M., J. G. Nurser, I. Stevens, and J. B. Sallée (2011), Subduction over the Southern Indian Ocean in a high-resolution atmosphere-ocean coupled model, *J. Climate*, *24*, 3830–3849.

Liu, J., T. Xiao, and L. Chen (2011), Intercomparisons of air-sea heat fluxes over the Southern Ocean, *J. Climate*, *24*(4), 1198–1211.

Lorenz, D. J., E. T. DeWeaver, and D. J. Vimont (2010), Evaporation change and global warming: The role of net radiation and relative humidity, *J. Geophys. Res.*, *115*, D20118, doi:10.1029/2010JD013949.

Lovenduski, N. S., and N. Gruber (2005), Impact of the Southern Annular Mode on Southern Ocean circulation and biology, *Geophys. Res. Lett.*, *32*(11), L11603, doi:10.1029/2005GL022727.

McCartney, M. S. (1977), Subantarctic mode water, in *A Voyage of Discovery, George Deacon 70th anniversary volume*, edited by M. V. Angel, Supplement to Deep-Sea Research, pp. 103–119, Pergamon Press, Oxford.

Meijers, A. J. S., E. Shuckburgh, N. Bruneau, J. B. Sallée, T. J. Bracegirdle, and Z. Wang (2012), Representation of the Antarctic circumpolar current in the CMIP5 climate models and future changes under warming scenarios, *J. Geophys. Res.*, *117*, C12008, doi: 10.1029/2012JC008412.

Meinshausen, M., et al. (2011), The RCP greenhouse gas concentrations and their extensions from 1765 to 2300, *Clim. Change*, *109*, 213–241.

Mellor, G., and A. Blumberg (2004), Wave breaking and ocean surface layer thermal response, *J. Phys. Ocean.*, *34*, 693–698.

Merryfield, W. J., G. Holloway, and A. E. Gatgett (1999), A global ocean model with double-diffusive mixing, *J. Phys. Ocean.*, *29*, 1124–1142.

Moore, J K., M. R. Abbott, and J. G. Richman (1999), Location and dynamics of the Antarctic Polar Front from satellite sea surface temperature data, *J. Geophys. Res.*, *104*(C2), 3059–3073.

Noh, Y., and H. S. Min (2004), Large eddy simulation of the ocean mixed layer: The effects of wave breaking and Langmuir circulation, *J. Phys. Ocean.*, *34*, 720–735.

Ridgway, K. R., J. R. Dunn, and J. L. Wilkin (2002), Ocean interpolation by four-dimensional weighted least squares: Application to the waters around Australasia, *J. Atmos. Ocean. Tech.*, *19*, 1357–1375.

Rintoul, S. R., and M. H. England (2002), Ekman transport dominates local air-sea fluxes in driving variability of Subantarctic Mode Water, *J. Phys. Ocean.*, *32*, 1308–1321.

Sabine, C., et al. (2004), The oceanic sink for anthropogenic CO_2, *Science*, *305*, 367–371.

Sallée, J. B., N. Wienders, K. Speer, and R. Morrow (2006), Formation of subantarctic mode water in the southeastern Indian Ocean, *Ocean Dyn.*, *56*(5), 525–542.

Sallée, J. B., R. Morrow, and K. Speer (2008a), Eddy heat diffusion and Subantarctic Mode Water formation, *Geophys. Res. Lett.*, *35*(5), L05607, doi:10.1029/2007GL032827.

Sallée, J. B., K. Speer, and R. Morrow (2008b), Response of the Antarctic Circumpolar Current to atmospheric variability, *J. Climate*, *21*, 3020–3039.

Sallée, J. B., K. Speer, S. Rintoul, and S. Wijffels (2010a), Southern Ocean thermocline ventilation, *J. Phys. Ocean.*, *40*(3), 509–529.

Sallée, J. B., K. G. Speer, and S. R. Rintoul (2010b), Zonally asymmetric response of the Southern Ocean mixed-layer depth to the Southern Annular Mode, *Nat. Geosci.*, *3*(4), 273–279.

Sallée, J. B., R. Matear, S. R. Rintoul, and A. Lenton (2012), Localised subduction of anthropogenic carbon dioxide in the Southern Hemisphere oceans, *Nat. Geosci.*, *5*, 579–584.

Sallée, J. B., E. Shuckburgh, N. Bruneau, A. Meijers, Z. Wang, T. Bracegirdle, and T. Roy (2013), Assessment of Southern Ocean water mass circulation in CMIP5 models: historical bias and forcing response, *J. Geophys. Res.,* doi:10.1002/jgrc.20135. in press.

Sarmiento, J. L., N. Gruber, M. A. Brzezinski, and J. P. Dunne (2004), High-latitude controls of thermocline nutrients and low latitude biological productivity, *Nature*, *427*, 56–60.

Séférian, R., D. Iudicone, L. Bopp, T. Roy, and G. Madec (2012), Water mass analysis of effect of climate change on air-sea CO2 fluxes: The Southern Ocean, *J. Climate*, *25*(11), 3894–3908.

Sloyan, B., and I. V. Kamenkovich (2007), Simulation of Subantarctic mode and Antarctic intermediate waters in climate models, *J. Climate*, *20*, 5061–5080.

Son, S. W., L. M. Polvani, D. W. Waugh, H. Akiyoshi, R. Garcia, D. Kinnison, S. Pawson, E. Rozanov, T. G. Shepherd, and K. Shibata (2008), The impact of stratospheric ozone recovery on the Southern Hemisphere westerly jet, *Science*, *320* (5882), 1486–1489, doi: 10.1126/science.1155939.

Son, S. W., E. P. Gerber, J. Perlwitz, L. M. Polvani, and co-authors (2010), Impact of stratospheric ozone on Southern Hemisphere circulation change: A multimodel assessment, *J. Geophys. Res.*, *115*, D00M07

Stommel, H. (1979), Determination of water mass properties of water pumped down from the Ekman layer to the geostrophic flow below, *Proc. Natl. Acad. Sci. U. S. A*, *76*(7), pp. 3051–3055.

Talley, L. D. (1999), Some aspects of ocean heat transport by the shallow, intermediate and deep overturning circulations, *Geophys. Mono. Ser.*, *112*, 1–22.

Taylor, K. E., R. J. Stouffer, and G. A. Meehl (2012), An overview of CMIP5 and the experiment design, *Bull. Am. Meteorol. Soc.*, *93*, 485–498.

Toggweiler, J., and J. Russell (2008), Ocean circulation in a warming climate, *Nature*, *45*, 286–288.